SANDIA REPORT

SAND2005-2021
Unlimited Release
Printed April 2005

An Analytical and Computational Study of Combined Rate and Size Effects on Material Properties

H. Eliot Fang, Zhen Chen, Luming Shen and Yong Gan

Prepared by
Sandia National Laboratories
Albuquerque, New Mexico 87185 and Livermore, California 94550

Sandia is a multiprogram laboratory operated by Sandia Corporation,
a Lockheed Martin Company, for the United States Department of Energy's
National Nuclear Security Administration under Contract DE-AC04-94AL85000.

Issued by Sandia National Laboratories, operated for the United States Department of Energy by Sandia Corporation.

Available to DOE and DOE contractors from
U.S. Department of Energy
Office of Scientific and Technical Information
P.O. Box 62
Oak Ridge, TN 37831

Telephone: (865)576-8401
Facsimile: (865)576-5728
E-Mail: reports@adonis.osti.gov
Online ordering: http://www.osti.gov/bridge

Available to the public from
U.S. Department of Commerce
National Technical Information Service
5285 Port Royal Rd
Springfield, VA 22161

Telephone: (800)553-6847
Facsimile: (703)605-6900
E-Mail: orders@ntis.fedworld.gov
Online order: http://www.ntis.gov/help/ordermethods.asp?loc=7-4-0#online

SAND2005-2021
Unlimited Release
Printed May 2005

An Analytical and Computational Study of Combined Rate and Size Effects on Material Properties

Zhen Chen, Luming Shen and Yong Gan

Department of Civil and Environmental Engineering

University of Missouri-Columbia, Columbia, MO 65211-2200

And

H. Eliot Fang

Computational Materials & Molecular Sciences Department

Sandia National Laboratories, PO Box 5800, Albuquerque, New Mexico 87185-1411

Abstract

The recent interests in developing multiscale model-based simulation procedures have brought about the challenging tasks of bridging different spatial and temporal scales within a unified framework. However, the research focus has been on the scale effect in the spatial domain with the loading rate being assumed to be quasi-static. Although material properties are rate-dependent in nature, little has been done in understanding combined loading rate and specimen size effects on the material properties at different scales. In addition, the length and time scales that can be probed by the molecular level simulations are still fairly limited due to the limitation of computational capability. Based on the experimental and computational capabilities available, therefore, an attempt is made in this report to formulate a hyper-surface in both spatial and temporal domains to predict combined size and rate effects on the mechanical properties of engineering materials. To demonstrate the features of the proposed hyper-surface, tungsten specimens of various sizes under various loading rates are considered with a focus on the uniaxial loading path. The mechanical responses of tungsten specimens under other loading paths are also explored to better understand the size effect. It appears from the preliminary results that the proposed procedure might provide an effective means to bridge different spatial and temporal scales in a unified multiscale modeling framework, and facilitate the application of nanoscale research results to engineering practice.

Acknowledgments

This work was sponsored in part by Sandia National Laboratories and the NSF-NIRT program. Sandia is a multiprogram laboratory operated by Sandia Corporation, a Lockheed Martin Company, for the United States Department of Energy's National Nuclear Security Administration under contract DE-AC04-94AL85000.

Contents

Figures

Tables

1. Introduction

As can be seen from the open literature, much research has been conducted to investigate the rate-dependence and size-dependence of material properties, respectively. However, the focus has been on the scale effect in the spatial domain with the loading rate being assumed to be quasi-static, as shown by the representative references [Bazant, 2002; Bazant and Chen, 1997; Gao et al., 1999; Huang et al., 2000; Su et al., 2003; among others]. The recent interests in developing multiscale model-based simulation procedures [Chen and Mehraeen, 2004; Fish and Chen, 2004; Qian et al., 2004; among others] have brought about the challenging tasks of bridging different spatial and temporal scales within a unified framework. Although material properties are rate-dependent in nature, little has been done in understanding combined loading rate and specimen size effects on the material properties at different scales.

On the other hand, the molecular level investigations have been conducted recently to explore the rate effect, the size effect, and the mechanical responses of thin films [Espinosa and Prorok, 2003; Horstemeyer et al., 2001a and b; Liang and Zhou, 2003; Shen and Chen, 2004; among others]. However, the length and time scales that can be probed by the molecular level simulations are still fairly limited due to the limitation of computational capability. A non-trivial question therefore arises: Can the current experimental facilities allow us to verify the molecular level simulation results? As can be found from the open literature related to the impact mechanics and shock physics [Brar and Bless, 1992; Camacho and Ortiz, 1996; Chen et al., 2003; Graham, 1993; Heuze, 1990; Zukas et al., 1992; among others], not only the loading rate but also the specimen size used in the current molecular dynamics (MD) simulation can not be handled by the existing experimental techniques. Usually, a specimen of finite size is employed in the bar and plate impact experiments to investigate the rate-dependent mechanical properties under the loading rate which is way below that used in the MD simulation reported so far.

Based on the experimental and computational capabilities available, hence, an attempt is made in this report to formulate a hyper-surface in both spatial and temporal domains to model combined size and rate effects on the mechanical properties of engineering materials. To demonstrate the features of the proposed hyper-surface, tungsten specimens of various sizes under various loading rates are considered with a focus on the uniaxial loading path. The mechanical responses of tungsten specimens under other loading paths are also explored to better understand the size effect. It appears from the preliminary results that the proposed procedure might provide an effective means to bridge different spatial and temporal scales in a unified multiscale modeling framework, and facilitate the application of nanoscale research results to engineering practice.

2. Formulation of a Hyper-Surface in Spatial and Temporal Domains

As shown in an asymptotic scaling analysis without considering the rate effect [Bazant, 2002], the relationship between the nominal strength σ_N and different sizes D of geometrically similar structures exhibits a two-sided asymptotic support, namely, the small-size asymptotic limit and large-size asymptotic limit, in the $log\, D - log\, \sigma_N$ space. Hence, a simple set of equations could be chosen to represent the size effect on the quasi-static strength σ_0 in the spatial domain, as follows:

$$\begin{cases} \sigma_0 = \sigma_u & D \le D_u \\ \log \sigma_0 = \log \sigma_m + (\log \sigma_u - \log \sigma_m)\left[1 - \sin\left(\dfrac{\pi}{2}\dfrac{\log D - \log D_u}{\log D_m - \log D_u}\right)\right] & D_u < D < D_m \\ \sigma_0 = \sigma_m & D_m \le D \end{cases}$$

where D_u is the specimen size at which the ultimate strength (ideal strength) σ_u is reached, and D_m the minimum macro-scale size beyond which the strength σ_m becomes size-independent. As can be seen from Eq. (1), the slope of the size-dependent portion with $D_u < D < D_m$ is given by:

$$\frac{d(\log \sigma_0)}{d(\log D)} = -\frac{\pi}{2}\frac{(\log \sigma_u - \log \sigma_m)}{(\log D_m - \log D_u)}\cos\left(\frac{\pi}{2}\frac{\log D - \log D_u}{\log D_m - \log D_u}\right)$$

which can be normalized to be

$$\frac{d(\log \sigma_0)}{d(\log D)} \Big/ \frac{(\log \sigma_u - \log \sigma_m)}{(\log D_m - \log D_u)} = -\frac{\pi}{2}\cos\left(\frac{\pi}{2}\frac{\log D - \log D_u}{\log D_m - \log D_u}\right)$$

As can be found from Eq. (3), the normalized slope could be fully determined with the small-size asymptotic limit and large-size asymptotic limit, and is in the range between $-\dfrac{\pi}{2}$ and zero. Although the question on a reasonable small-size asymptotic limit remains open [Bazant, 2002], the proposed formulation might provide a simple means to characterize the size-dependence of certain materials under quasi-static loading conditions.

To describe the dependence of the material strength on the strain rate $\dot{\varepsilon}$, a simple model proposed by Cowper and Symonds [1957] is adopted as follows:

$$\frac{\sigma(\dot{\varepsilon})}{\sigma_o} = 1 + \left(\frac{\dot{\varepsilon}^p}{\dot{\varepsilon}_r} \right)^{1/q}$$

in which $\dot{\varepsilon}^p$ denotes the plastic strain rate, σ_o is the quasi-static strength, and $\dot{\varepsilon}_r$ and q are two model parameters that can be determined with two experimental data points of $\sigma(\dot{\varepsilon})$. The size effect on the model parameters are not considered in the original model. As compared with the plastic strain, the elastic strain can be neglected so that $\dot{\varepsilon}^p = \dot{\varepsilon}$ could be assumed. As shown by Horstemeyer et al. [2001a and b], however, there exists a critical strain rate for single-crystal metals, below which the material strength becomes rate-independent. The critical strain rate is increased with the decrease of the specimen size. In other words, the model parameters $\dot{\varepsilon}_r$ and q in Eq. (4) could be assumed to be size-dependent if this model is used to predict the rate-dependent strength with the strain rate above the critical strain rate. Thus, a three-dimensional hyper-surface with respect to both spatial and temporal domains could be formulated to describe combined size and rate effects on the material strength, as below.

Based on Eq. (4), the hyper-surface is assumed to have a two-sided asymptotic support, namely, the small-size asymptotic limit and large-size asymptotic limit, in the $\log\frac{\sigma - \sigma_o}{\sigma_o} - \log\frac{\dot{\varepsilon}}{\dot{\varepsilon}_r}$ space. The small-size asymptotic limit and large-size asymptotic limit are represented by $(\dot{\varepsilon}_{rs}, \sigma_{os}, q_s)$ and $(\dot{\varepsilon}_{rl}, \sigma_{ol}, q_l)$, respectively, which can be determined by continuum and molecular level studies. The size dependence of model parameters $\dot{\varepsilon}_r$ and q can therefore be described as follows:

$$\frac{\log\dot{\varepsilon}_r - \log\dot{\varepsilon}_{rl}}{\log\dot{\varepsilon}_{rs} - \log\dot{\varepsilon}_{rl}} = 1 - \sin\left(\frac{\pi}{2} \frac{\log D - \log D_{rs}}{\log D_{rl} - \log D_{rs}} \right)$$

$$\frac{q - q_l}{q_s - q_l} = 1 - \sin\left(\frac{\pi}{2} \frac{\log D - \log D_{rs}}{\log D_{rl} - \log D_{rs}} \right)$$

for $D_{rs} < D < D_{rl}$ with D_{rs} and D_{rl} being the specimen sizes at the small-size asymptotic limit and large-size asymptotic limit, respectively. For $D \geq D_{rl}$, we have $\dot{\varepsilon}_r = \dot{\varepsilon}_{rl}$ and $q = q_l$, while for $D \leq D_{rs}$, we have $\dot{\varepsilon}_r = \dot{\varepsilon}_{rs}$ and $q = q_s$. It follows from Eqs. (4) and (5) that the three-dimensional hyper-surface takes the form of

$$\sigma(\dot{\varepsilon}, D) = \sigma_o(D)\left[1 + 10^{**}\left(\frac{1}{q(D)} \left(\log\dot{\varepsilon} - \log\dot{\varepsilon}_r(D) \right) \right) \right]$$

or

$$\log\sigma(\dot{\varepsilon},D)=\log\sigma_o(D)+\log\left[1+10^{**}\left(\frac{1}{q(D)}(\log\dot{\varepsilon}-\log\dot{\varepsilon}_r(D))\right)\right]$$

in the $\log\dot{\varepsilon}-\log D-\log\sigma$ space. In Eq. (6) or (7), $\dot{\varepsilon}_r(D)$ and $q(D)$ are determined from Eq. (5), and $\sigma_0(D)$ is defiend by Eq. (1) because the size-dependent quasi-static strength is rate-independent. To characterize the hyper-surface, integrated molecular and continuum investigations must be performed to determine the small-size asymptotic limit and large-size asymptotic limit, as demonstrated in the next section.

3. Demonstration and Discussion

Based on the recent research results on multiscale model-based simulation of tungsten (W) thin film delamination from silicon substrate [Chen et al., 2004; Shen and Chen, 2004], combined loading rate and specimen size effects on the mechanical properties of W are explored with the use of the proposed hyper-surface. The MD simulation is performed first to find the small-size asymptotic limit, and the existing continuum level data are employed to determine the large-size asymptotic limit.

To determine the small-size asymptotic limit, the computational set-up for the MD simulation of single-crystal W specimen under uniaxial tensile loading is shown in Figure 1. The three-dimensional simulation super-cell consists of two parts. One part is referred to as the active zone in which the atoms move according to the interactions among the neighboring atoms; the other part, wrapped by the boxes as presented in Figure 1, is referred to as the boundary zone where the atoms are assigned a fixed rigid body velocity. The dimension of active zone is indicated by H, D and W, while the size of each boundary zone in the z-direction is $2a_o$ with a_o being the lattice parameter of W. The crystal orientation of (x[1 0 0], y[0 1 0], z[0 0 1]) is considered with the periodic boundary condition (PBC) being imposed along both the x- and y-directions.

In the simulation, all atoms are initially placed at their equilibrium positions at the temperature of 298 K. Those atoms in the boundary zone are then fixed. After the system has equilibrated for a certain period, constant velocities with the same magnitude and opposite direction are assigned to the atoms in the top and bottom boundary zones, respectively, to simulate a displacement-controlled uniaxial tensile loading in the z-direction. A velocity scaling technique is employed to maintain a constant temperature of 298 K. The Embedded Atom Method (EAM) developed by Daw and Baskes [1984] is used to model the interatomic potential among W atoms. The corresponding model parameters for W are based on the work of Zhang and Ouyang [1993]. The method applied to integrate the equations of motion is the 6-value Gear predictor-corrector algorithm. The largest time step size that can keep the total system energy remaining constant in the adiabatic simulation for the motion of W atoms with the EAM potential is used in the numerical study. A time step size of 0.5 fs is chosen after performing several adiabatic simulations for the W atoms at different initial temperatures up to 2000 K.

Stress calculation in the MD simulations has been the focus of many investigations over the past years. In this study, the formulations employed to calculate atomic-level stresses are motivated by the work of Zhou [2003]. At each atom, the local stress tensor is defined to be

$$\boldsymbol{\beta}_i = -\frac{1}{\Omega_i}\sum_{j>i}^{N^n} \boldsymbol{f}_{ij} \otimes \boldsymbol{r}_{ij}$$

in which i refers to the atom considered and j refers to the neighboring atom, rij is the position vector between atoms i and j, Nn is the number of neighboring atoms surrounding i, and fij is the force vector on atom i due to atom j. The global continuum stress tensor is then determined by atom *i*, Ω_i is the volume of atom

$$\boldsymbol{\sigma} = \frac{1}{N^*} \sum_{i}^{N^*} \boldsymbol{\beta}_i$$

where N* represents the total number of atoms in a representative volume of continuum. Since the W block is under very large deformation, true strain ε is used in this study with $\varepsilon = ln\left(\frac{L}{L_0}\right)$ where Lo and L are the original and deformed lengths of the specimen, respectively.

To study the effects of specimen size and strain rate on the mechanical responses of single crystal W block under uniaxial tensile loading, seven MD simulation cases are designed, as specified in Table 1. By introducing different number of defects in Simulation 2, the effect of the vacancies in the W specimen on the stress-strain relation is also investigated to better understand the size effect.

3.1. The Effect of Specimen Size

To study the effect of specimen size on the tensile deformation of single crystal W, Simulations 1-5 are performed. Figure 2 shows the corresponding stress-strain curves of different W blocks under tensile loading. As can be seen from the figure, the initial elastic modulus of W is almost independent on the specimen size. However, the peak stress increases as the specimen size decreases, which is mainly due to the fact that larger specimens offer more spaces for dislocation to occur. Although there exist the constraints due to the boundary zones and the PBC used in the simulations, the single crystal W specimen is a discrete system with atoms distributed only at certain positions. The bonds among atoms are the relatively weak parts while the individual atoms are the strong parts of the system. The increase of specimen size increases the number of relatively weak bonds, which in turn offers more possibilities for bond breaking and dislocation to occur, and thus reduces the strength of the specimen.

3.2. The Effect of Defects

To verify the above claim that the decrease of the W strength with the increase of specimen size is mainly due to the fact that larger specimens provide more spaces for dislocation to occur, the effect of artificially introduced defects in a single crystal W block on the stress-strain relation is investigated. Different numbers of vacancies are introduced into Simulation 2 with other simulation conditions being kept the same. The stress-strain curves of W blocks with zero, one, two and four vacancies distributed in the same *x-y* plane which is initially located 2.152 nm away from the top end of the active

zone are presented in Figure 3. As can be seen from the figure, all the stress-strain curves are initially the same until failure occurs. The strength of W decreases as the number of vacancies increases, since more vacancies offer more possibilities for bond breaking and dislocation to occur. However, the rate of decrease in strength slows down when vacancies become saturated. To study the effect of the vacancy distribution in the *z*-direction on the stress-strain relation, four cases with zero, one, two and four vacancies, respectively, located at the center of *x*-*y* plane but different positions in the *z*-direction, are considered with other simulation conditions being kept the same as those in Simulation 2. The corresponding stress-strain curves are similar to those as shown in Fig. 3. Hence, it appears that the increase of the number of defects regardless of the distribution position in a single crystal W block would increase the possibility for dislocation to occur and thus reduce the strength of W, which is similar to the effect of increasing specimen size on the strength of W. Therefore, it is reasonable to conclude that larger single-crystal specimens provide more spaces for dislocation to occur which in turn reduces the strength of W.

3.3 The Effect of Strain Rate

To investigate the effect of the tensile strain rate on the stress-strain relation of a single-crystal W specimen at the atomic level, Simulations 4, 6 and 7 are performed with the initial strain rate being 2×10^{9} s^{-1}, 2×10^{8} s^{-1} and 2×10^{10} s^{-1}, respectively. Figure 4 illustrates the corresponding stress-strain curves. As can be observed from the figure, the initial elastic modulus of W is insensitive to the strain rate, but the peak stress increases with the strain rate. The dependence of peak stress on the strain rate is mainly due to the dynamic wave effect that impedes the motion of dislocations [Liang and Zhou, 2003]. Note that the rate-dependence of peak stress becomes weak with the decrease of the strain rate. In other words, there is a critical strain rate for single-crystal metals, below which the material strength becomes rate-insensitive. As shown by Horstemeyer et al. [2001a and b], the critical strain rate is increased with the decrease of the specimen size. Hence, the size-dependent quasi-static strength, as described by Eq. (1), could be estimated with the current MD simulation capability if the specimen size is at the nanoscale, which makes it feasible to evaluate the small-size asymptotic limit.

3.4 Determination of the Hyper-Surface for Tungsten

Based on the work of Horstemeyer et al. [2001a and b], it can be assumed that the strength of W obtained at the strain rate of 2×10^{8} s^{-1} is closed to the quasi-static strength at the given specimen size used in Simulation 6. As can be observed from Fig. 4, the strength of W decreases from 24.8 GPa at the rate of 2×10^{9} s^{-1} in Simulation 4 to 22.2 GPa at the rate of 2×10^{8} s^{-1} in Simulation 6, with a factor of 22.2/24.8 = 0.895. For the sake of simplicity, therefore, all the strengths obtained in Simulations 1-5 with the strain rate of 2×10^{9} s^{-1} are multiplied by a factor of 0.895 to get the approximate quasi-static strengths at different spatial scales. Since the specimen sizes used in Simulations 1-3 are less than those used in Simulations 4-7, this treatment should result in a reasonable ideal strength because the critical strain rate is increased with the decrease of the specimen size.

Indentation tests on single crystal W have shown that the material hardness depends on the specimen size but the indents with diagonals being longer than about 100 μm cease to display any hardness-dependence on the size [Hutchinson, 2000]. Since the material hardness is directly related to the strength, $D_m = 100\mu m$ and $\sigma_m = 1.5GPa$ can be used in Eq. (1). With the use of the MD simulation results, hence, the size-dependent quasi-static strength can be determined as shown in Fig. 5. As can be seen, $\sigma_u = 34.9GPa$ at $D_u = 1.6nm$ could be chosen for Eq. (1), which is in a good agreement with the ideal tensile strength of 29.5 GPa as reported by Roundy et al. [2001] using pseudopotential density functional theory. Thus, the multiscale quasi-static strength of W, as described by Eq. (1), could be shown in Fig. 5.

To determine the hyper-surface in both spatial and temporal domains, as described by Eqs. (1), (5) and (7), the small-size asymptotic limit and large-size asymptotic limit, namely, $(\dot{\varepsilon}_{rs}, \sigma_{os}, q_s)$ and $(\dot{\varepsilon}_{rl}, \sigma_{ol}, q_l)$, must be obtained via integrated molecular and continuum level studies. As shown in the experimental study at continuum level [Zurek et al., 1992], the strength of W is sensitive to the strain rate so that two data points, $(2.0GPa, 2000.0s^{-1})$ and $(1.6GPa, 1.0s^{-1})$, could be taken to get

$$\dot{\varepsilon}_{rl} = 3.6e5s^{-1} \qquad \text{and} \qquad q_l = 4.7 \qquad \text{at} \qquad D_{rl} = 100\mu m$$

based on Eq. (4), and with the use of $\sigma_{ol} = \sigma_m = 1.5GPa$. Based on the MD simulation results presented above, the small-size asymptotic limit can be found via Eq. (1) and $\sigma_{os} = 22.2GPa$ at $\dot{\varepsilon} = 2.0e8s^{-1}$ and $D = 3.2nm$, as follows:

$$\dot{\varepsilon}_{rs} = 5.3e11s^{-1} \qquad \text{and} \qquad q_s = 2.6 \qquad \text{at} \qquad D_{rs} = 3.2nm$$

for which the two data points, $(24.8GPa, 2.0e9s^{-1})$ and $(28.5GPa, 2.0e10s^{-1})$ at $D = 3.2nm$, have been employed. As a result, the hyper-surface for W can be determined as shown in Fig. 6. As can be seen, combined rate and size effects on the strength of W could be estimated with a two-sided asymptotic support. Although more data points are needed from multiscale studies to refine the hyper-surface, the proposed procedure might provide an effective means to bridge different spatial and temporal scales in a unified multiscale modeling framework.

It should be indicated that the combined rate and size effects on the mechanical responses of tungsten are different under various loading paths. To demonstrate this point, preliminary MD simulations have been performed to explore the size effect on the mechanical response of single-crystal W under pre-compressed shear loading, as shown in Fig. 7 for the computational set-up. Three specimens of different sizes are first compressed to 0, 0.33, 0.5 and 0.7 of the corresponding compressive strength, respectively, and are then tested under shear loading. As can be observed from Figs. 8-10, the degree of strength oscillation is increased with the decrease of specimen size before fracture occurs, which is different from the uniaxial loading case as shown in Fig. 2 under the same strain rate. The shear strength dependence on the pre-compression level is also

oscillating. It appears from the preliminary study that the rearrangement of lattice structure under pre-compressed shear loading is more pronounced than that under uniaxial tensile loading. However, both loading paths exhibit definite size effects on the strength of W.

4. Conclusions

Based on the current experimental and computational capabilities, an attempt has been made in this report to explore the effects of combined loading rates and specimen sizes, and to formulate a hyper-surface in both spatial and temporal domains to predict the combined size and rate effects on the mechanical properties of materials. With a two-sided asymptotic support, the proposed hyper-surface could be determined via integrated molecular and continuum level investigations. To demonstrate the features of the proposed procedure, tungsten specimens of various sizes under different loading rates are considered with a focus on the uniaxial loading path. The mechanical responses of tungsten specimens under pre-compressed shear loading paths are also explored to better understand the size effect. It appears from the preliminary results that the proposed procedure might provide an effective means to bridge different spatial and temporal scales in a unified multiscale modeling framework, and facilitate the application of nanoscale research results to engineering practice. An integrated experimental, analytical and computational effort is required to further improve the hyper-surface so that it could be applied to general cases.

5. References

1. Bazant, Z.P. (2002), "Scaling of Dislocation-Based Stain-Gradient Plasticity," *Journal of the Mechanics and Physics of Solids*, Vol. 50, pp. 435-448.

2. Bazant, Z.P., and Chen, E.P. (1997), "Scaling of Structural Failure," *Applied Mechanics Reviews*, Vol. 50**,** pp. 593-627.

3. Brar, N.S., and Bless, S.J. (1992), "Failure Waves in Glass under Dynamic Compression," *High Pressure Research*, Vol. 10, pp. 773-784.

4. Camacho, G.T., and Ortiz, M. (1996), "Computational Modeling of Impact Damage in Brittle Materials," *International Journal of Solids and Structures*, Vol. 33, pp. 2899-2938.

5. Chen, J.S., and Mehraeen, S. (2004), "Variationally Consistent Multiscale Modeling and Homogenization of Stressed Grain Growth," *Computer Methods in Applied Mechanics and Engineering*, Vol. 193, pp. 1825-1848.

6. Chen, Z., Feng, R., Xin, X., and Shen, L. (2003), "A Computational Model for Impact Failure with Shear-Induced Dilatancy," *International Journal for Numerical Methods in Engineering*, Vol. 56, pp. 1979-1997.

7. Chen, Z., Shen, L., Mai, Y.-W., and Shen, Y.G. (2004), "A Bifurcation-Based Decohesion Model for Simulating the Transition from Localization to Decohesion with the MPM, to appear in *Journal of Applied Mathematics and Physics (ZAMP)*.

8. Cowper, G.R., and Symonds, P.S. (1957), *Strain Hardening and Strain Rate Effects in the Impact Loading of Cantilever Beams*, Technical Report No. 28 (ONR Contract No. 562), Division of Engineering, Brown University, Providence, RI.

9. Daw, M.S., and Baskes, M.I. (1984), "Embedded-atom Method: Derivation and Application to Impurities," Surfaces, and Other Defects in Metals, *Physical Review Letter*, Vol. 29**,** pp. 6443-6453.

10. Espinosa, H.D., and Prorok, B.C. (2003), "Size Effects on the Mechanical Behavior of Gold Thin Films," *Journal of Materials Science*, Vol. 38, pp. 4125-4128.

11. Fish, J., and Chen, W. (2004), "Discrete-to-Continuum Bridging Based on Multigrid Principles," *Computer Methods in Applied Mechanics and Engineering*, Vol. 193, pp. 1693-1711.

12. Gao, H., Huang, Y., Nix, W.D., and Hutchinson, J.W. (1999), "Mechanism-Based Strain Gradient Plasticity – I. Theory," *Journal of the Mechanics and Physics of Solids*, Vol. 47, pp. 1239-1263.

13. Graham R.A. (1993), *Solids under High-Pressure Shock Compression*, Springer-Verlag.

14. Heuze, F.E. (1990), "An Overview of Projectile Penetration into Geological Materials, with Emphasis on Rocks," *International Journal of Rock Mechanics and Mining Sciences & Geomechanics Abstracts*, Vol. 27, pp. 1-14.

15. Horstemeyer, M.F., Baskes, M.I., and Plimpton, S.J. (2001a), "Computational Nanoscale Plasticity Simulations Using Embedded Atom Potentials," *Theoretical and Applied Fracture Mechanics*, Vol. 37, pp. 49-98.

16. Horstemeyer, M.F., Baskes, M.L., and Plimpton, S.J. (2001b), "Length Scale and Time Scale Effects on the Plastic Flow of FCC Metals," *Acta Materialia*, Vol. 49, pp. 4363-4374.

17. Huang, Y., Gao, H., Nix, W.D., and Hutchinson, J.W. (2000), "Mechanisms-Based Strain Gradient Plasticity – II. Analysis," *Journal of the Mechanics and Physics of Solids*, Vol. 48, pp. 99-128.

18. Hutchinson, J.W. (2000), "Plasticity at the Micron Scale," *International Journal of Solids and Structures*, Vol. 37, pp. 225-238.

19. Liang, W., and Zhou, M. (2003), "Size and Strain Rate in Tensile Deformation of Cu Nanowires," *Nanotech*, Vol. 2, pp. 452-455.

20. Qian, D., Wagner, G.J., and Liu, W.K. (2004), "A Multiscale Projection Method for the Analysis of Carbon Nanotubes, *Computer Methods in Applied Mechanics and Engineering*, Vol. 193, pp. 1603-1632.

21. Roundy, D., Krenn, C.R., Cohen, M. L., and Morris, J.W. (2001), "Ideal Strength of BCC Tungsten," *Philosophical Magazine A*, Vol. 81, pp. 1725-1747.

22. Su, H., Moran, B., Liu, W.K., and Olson, G.B. (2003), "A Hierarchical Multi-Physics Model for Design of High Toughness Steels," *Journal of Computer-Aided Materials Design*, Vol. 10, pp. 99-142.

23. Shen, L., and Chen, Z. (2004), "An Investigation of the Effect of Interfacial Atomic Potential on the Stress Transition in Thin Films," *Modeling and Simulation in Materials Science and Engineering*, Vol. 12, pp. S347-S369.

24. Zhang, B., and Ouyang, Y. (1993), "Theoretical Calculation of Thermodynamics Data for BCC Binary Alloys with the Embedded-Atom Method," *Physical Review B*, Vol. 48, pp. 3022-3029.

25. Zhou, M. (2003), "A New Look at the Atomic Level Virial Stress: on Continuum-Molecular System Equivalence," *Proceeding A of the Royal Society*, Vol. 459, pp. 2347-2392.

26. Zukas, J.A., Nicholas, T., Swift, H.F., Greszczuk, L.B., and Curran, D.R. (1992), *Impact Dynamics*, Krieger Publishing Company, Malabar, FL.

27. Zurek, A.K., Follansbee, P.S., and Kapoor, D. (1992), "Strain Rate and Temperature Effects in Tungsten and Tungsten Alloys," *High Strain Rate Behavior of Refractory Metals and Alloys*, Edited by R. Asfahani, E. Chen and A. Crowson, The Minerals, Metals and Materials Society, pp. 179-191

Appendix A: Tables & Figures

Table 1. Description of the MD simulation cases.

Simulation #	Specimen Size $D \times W \times H$ (nm^3)	Number of Active Atoms	Initial Strain Rate (s^{-1})	Peak Stress (GPa)
1	1.27 × 1.27 × 3.83	384	2×10^{9}	39.0
2	1.59 × 1.59 × 4.78	750	2×10^{9}	39.1
3	2.54 × 2.54 × 7.65	3,072	2×10^{9}	28.6
4	3.19 × 3.19 × 9.56	6,000	2×10^{9}	24.8
5	6.38 × 6.38 × 19.13	48,000	2×10^{9}	18.5
6	3.19 × 3.19 × 9.56	6,000	2×10^{8}	22.2
7	3.19 × 3.19 × 9.56	6,000	2×10^{10}	28.5

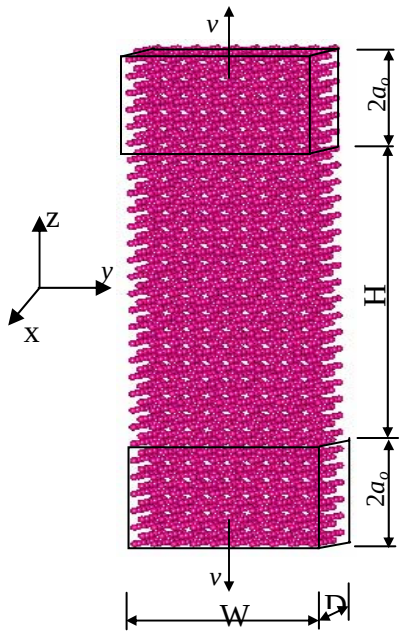

Figure 1: Computational model of single crystal W block under uniaxial tensile loading.

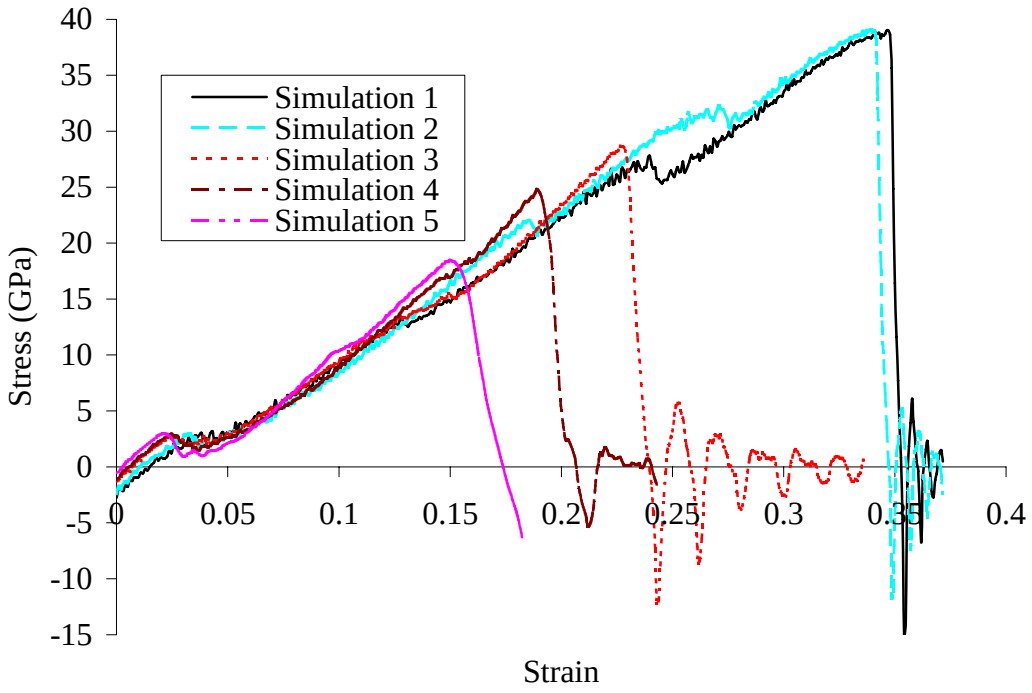

Figure 2: The size effect on the stress-strain curves of W under tensile strain rate of 2×10^{9} S^{-1}.

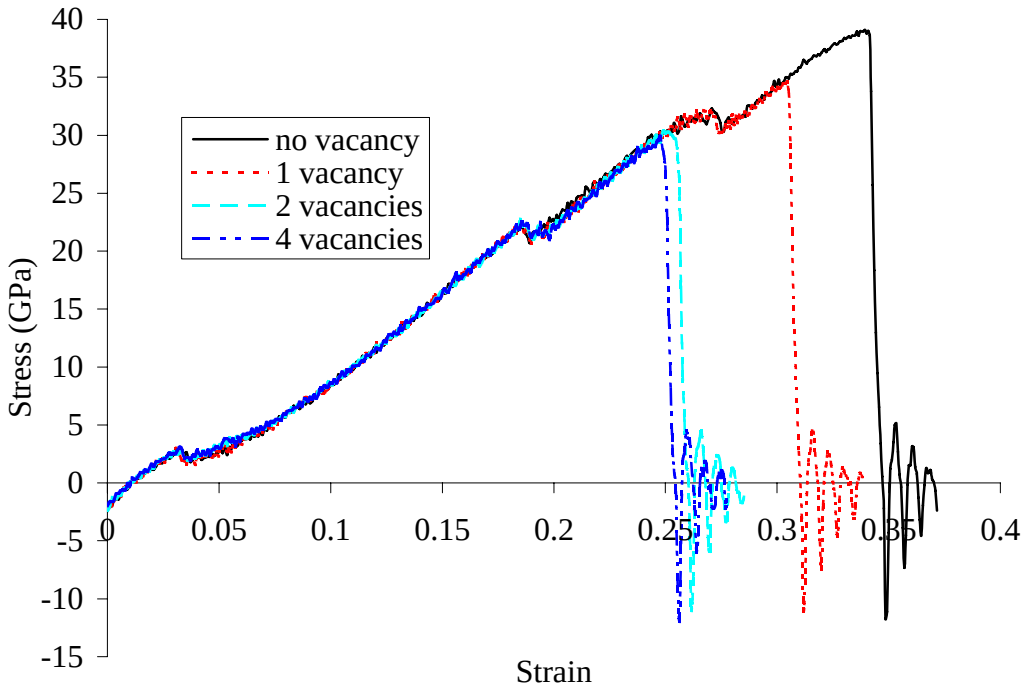

Figure 3: The effect of vacancies distributed in the same x-y plane on the stress-strain curves.

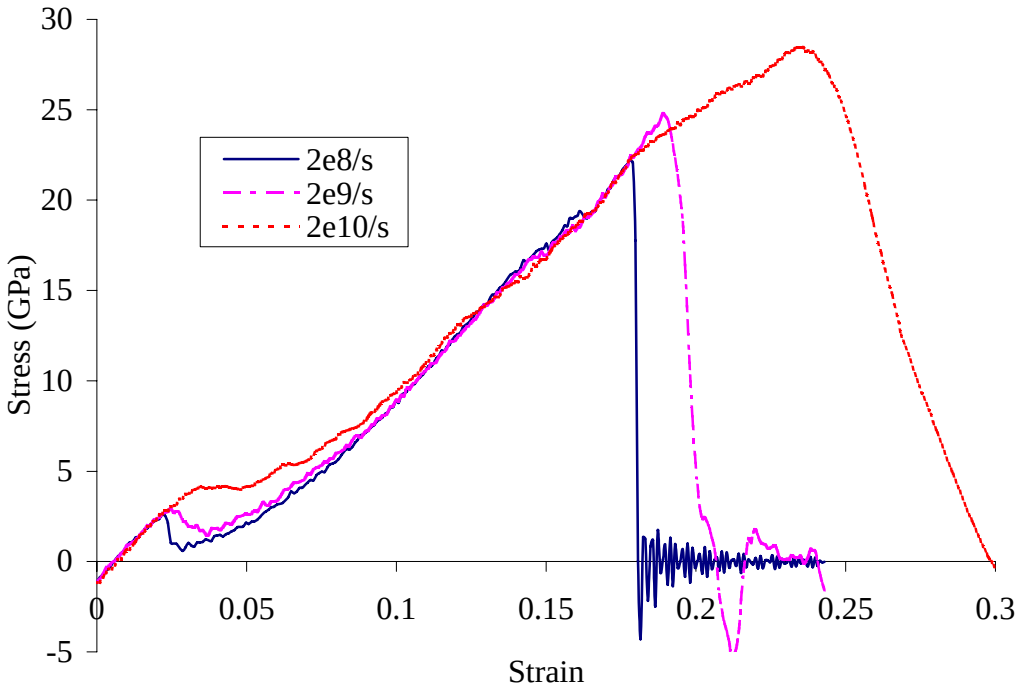

Figure 4: The effect of strain rate on the stress-strain curve of single-crystal W under tension.

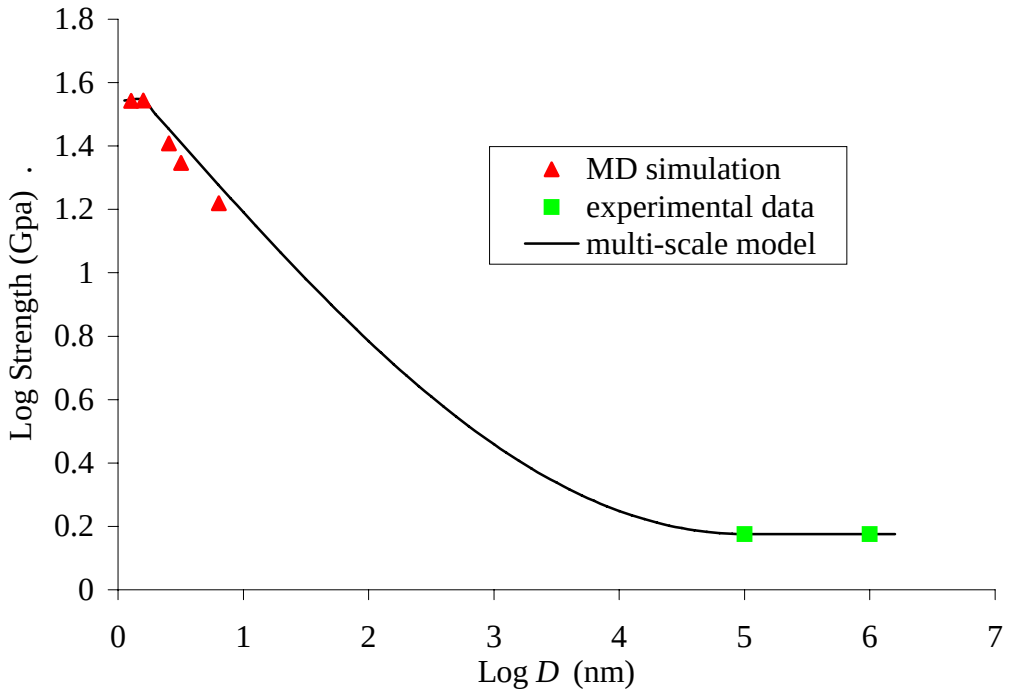

Figure 5: Size-dependent quasi-static strength of tungsten.

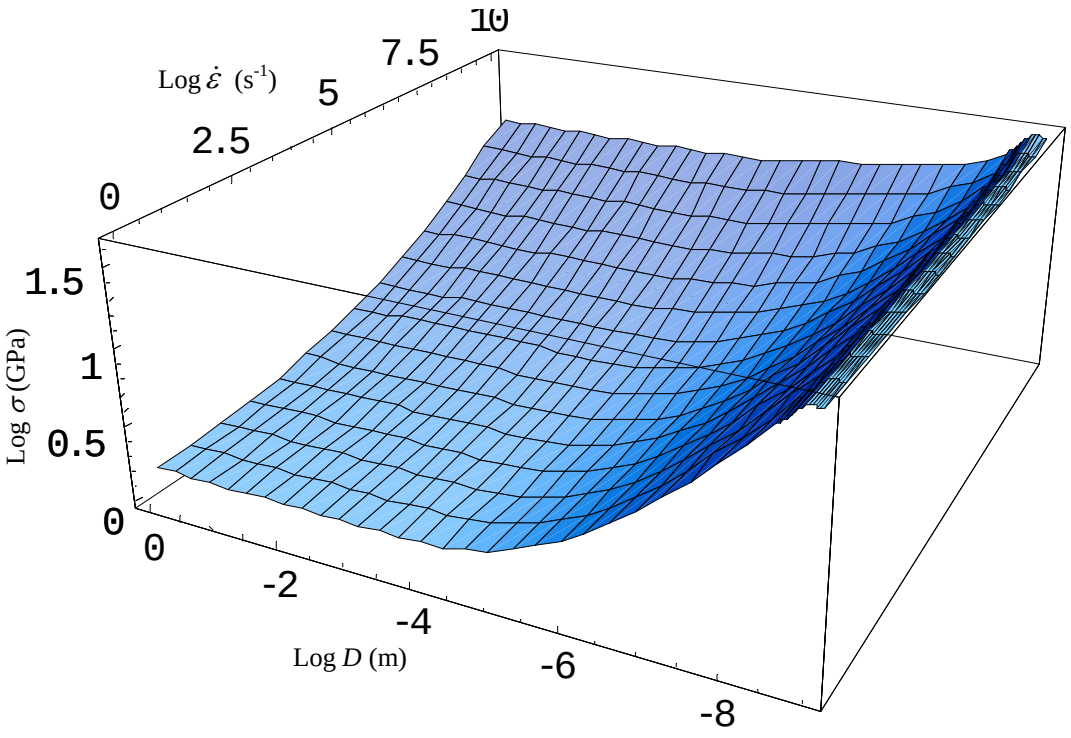

Figure 6: The hyper-surface for tungsten in both spatial and temporal domains.

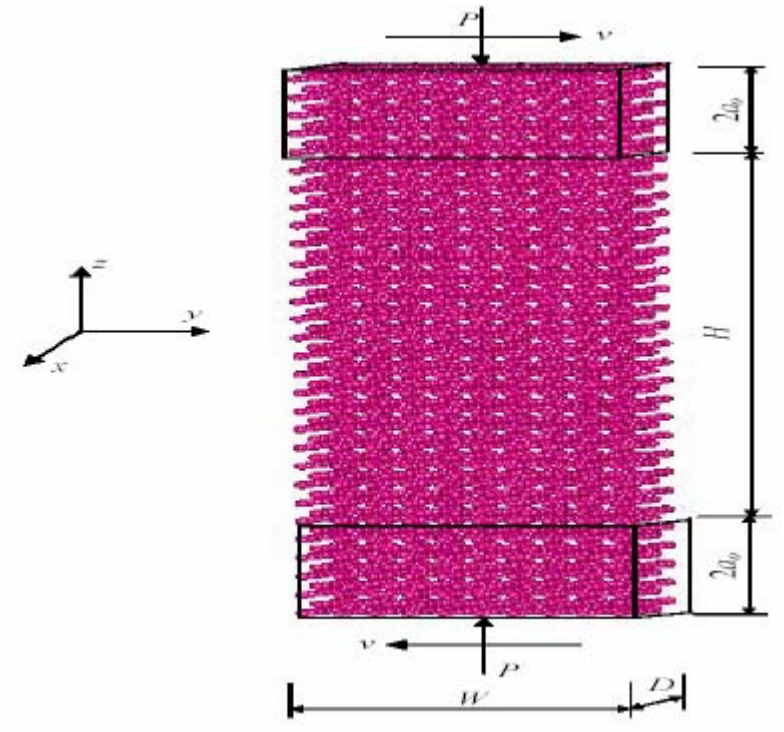

Figure 7: A pre-compressed tungsten single crystal with orientation of (x[100], y[010], z[001]) under simple shear strain rate of $2x10^9$ S^{-1} (periodic boundary conditions being applied along the x-direction).

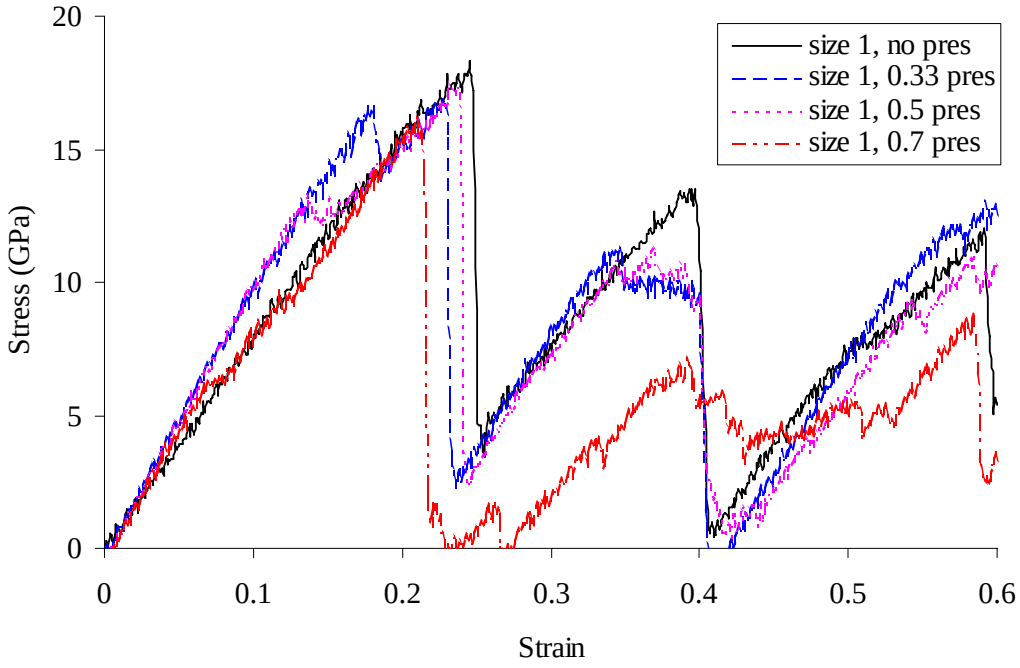

Figure 8: The effect of pressure on the W single crystals with size 1: $5a_o \times 10a_o \times 5a_o$.

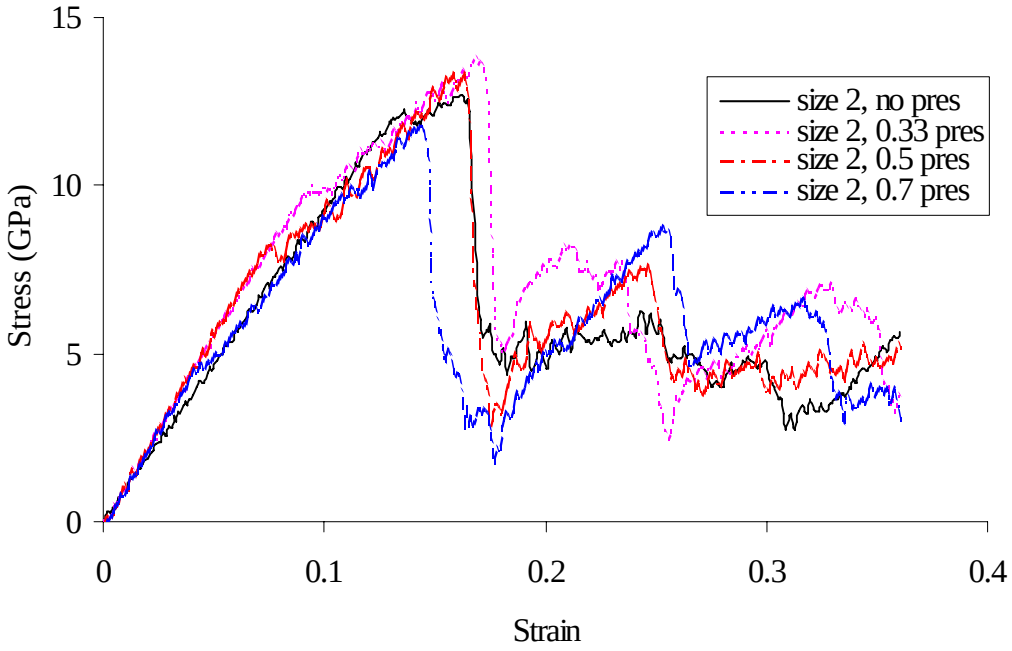

Figure 9: The effect of pressure on the W single crystals with size 2: $5a_o \times 20a_o \times 10a_o$.

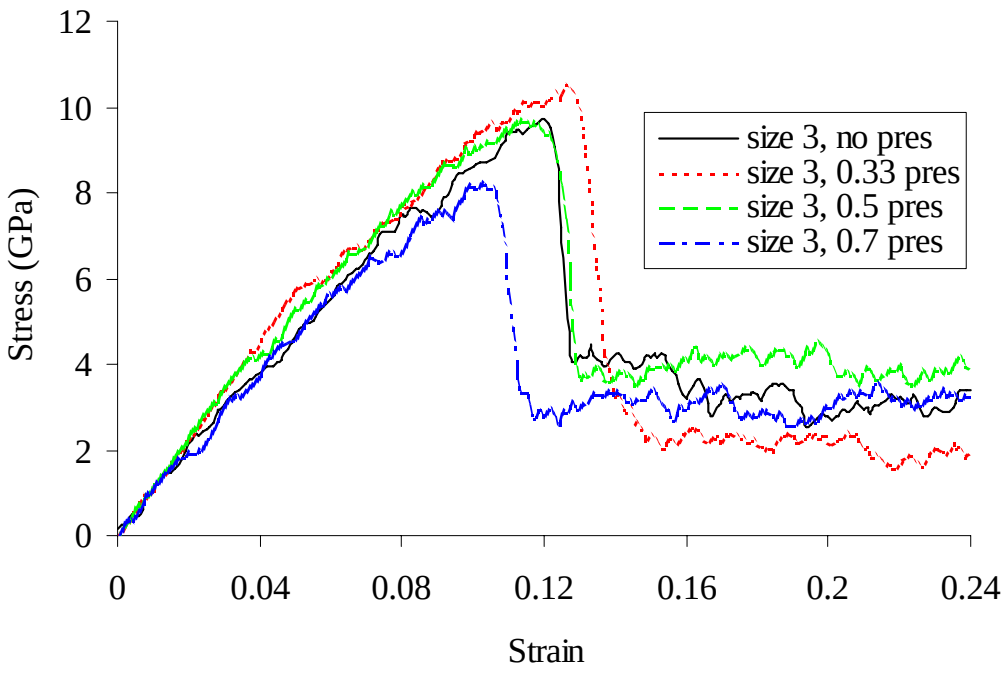

Figure 10: The effect of pressure on the W single crystals with size 3: $5a_o \times 40a_o \times 20a_o$.

Distribution:

2	MS0899	Technical Library	9616
1	MS1411	Corbett C. Battaile	1814
1	MS1411	Joanne L. Budzien	1814
1	MS1411	Michael E. Chandross	1814
1	MS1411	William A. Counts	1814
10	MS1411	H. Eliot Fang	1814
1	MS1411	Stephen M. Foiles	1814
1	MS1411	Amalie L. Frischknecht	1814
1	MS1411	David R. Heine	1814
1	MS1411	Elizabeth A. Holm	1814
1	MS1411	Jeffrey J. Hoyt	1814
1	MS1411	Ahmed Ismail	1814
1	MS1411	Koenraad F. Janssens	1814
1	MS1411	Veena Tikare	1814
1	MS1411	Frank B. van Swol	1814
1	MS1411	Edmund B. Webb	1814
1	MS9018	Central Technical Files	8945-1